

Target position estimation using frequency-hopping signals based on microwave photonic subsampling

Xiaohu Tang (汤晓虎), Cong Ma (马 丛), Kunlin Shao (邵琨麟), Yuxiang Cai (蔡宇翔), Ping Li (李 平), Yamei Zhang (张亚梅), and Shilong Pan (潘时龙)

National Key Laboratory of Microwave Photonics, Nanjing University of Aeronautics and Astronautics, Nanjing 210016, China

*Corresponding author: zhang_ym@nuaa.edu.cn

Received November 28, 2024 | Accepted February 17, 2025 | Posted Online June 5, 2025

A microwave photonic subsampling digital receiver (MPSDR) is proposed and experimentally demonstrated for target detection with a sampling rate of 10 MSa/s. Stepped and pseudo-random frequency-hopping signals with frequencies across the K band are both used for target detection and can be captured by the MPSDR. The range profiles of the targets are then derived using a compressed sensing algorithm, and precise target position estimation is achieved by changing the measurement position of the antenna pair. The results demonstrate that the estimation accuracy remains comparable even when the pseudo-random frequency-hopping signal utilizes only 12.5% of the frequency points required by the stepped frequency-hopping signal. This highlights the efficiency and potential of the proposed MPSDR in processing complex signals while maintaining high accuracy.

Keywords: microwave photonic subsampling; target positions estimation; frequency-hopping signal; compressed sensing. **DOI:** 10.3788/COL202523.073902

1. Introduction

Target position estimation is one key function of microwave radar, attracting extensive attention across diverse fields such as defense, autonomous vehicles, and environmental monitoring^[1]. Nevertheless, traditional radar waveforms used in position estimation are often prone to interference, which can severely undermine their effectiveness^[2,3]. In this context, frequency-hopping (FH) signals are widely employed in radar due to their strong anti-jamming capabilities^[4,5]. However, conventional digital receivers face substantial challenges in handling high-frequency FH signals, especially FH signals with complex hopping patterns due to inherent limitations in analog-to-digital converter (ADC) bandwidths, sampling rates, and associated costs^[6], thereby constraining their practical applications in high-frequency and highly complex signal processing.

Microwave photonic subsampling digital receivers (MPSDRs) present a transformative alternative for high-frequency signal processing, offering numerous advantages such as ultrawide bandwidth, low jitter, and high sampling accuracy^[7,8]. These receivers have demonstrated remarkable potential in microwave signal parameter measurements, including frequency measurement^[9,10] and signal position estimation^[11]. However, prior implementations of MPSDRs have largely relied on multiple mode-locked lasers (MLLs) or modulators, resulting in increased system complexity and cost. Moreover, in the realm of target position estimation, no reported studies have explored

the direct sampling and processing of FH signals using the MPSDR. Therefore, a low-complexity MPSDR for FH signals needs to be developed to fully exploit its potential advantages.

In this Letter, a simple-structured MPSDR based on a dualpolarization dual-drive Mach-Zehnder modulator (DP-DMZM) is proposed and employed for FH signal processing with a sampling rate of 10 MSa/s. The proposed MPSDR can directly sample and process high-frequency FH signals using low-speed, ultralow-jitter optical pulses and thus convert them to baseband signals, significantly reducing the bandwidth and sampling rate requirements of electronic components. Furthermore, the proposed MPSDR can be adapted to varied hopping patterns, which expands the applicability of the system. Range profile detection and target position estimation are achieved by extracting the target responses. A frequency grid ranging from 18.001 to 26.001 GHz, with 10 MHz intervals, is used for frequency hopping. The range profile detection is first demonstrated using a stepped frequency-hopping signal (SFHS) with 801 hops. Then, a pseudo-random frequency-hopping signal (PRFHS) with 100 hops is performed. The range profile is successfully reconstructed by solving an l_1 minimization problem based on the target responses corresponding to the 100 hopped frequencies. The results indicate that the accuracy of the range profile remains comparable, although the PRFHS uses only 12.5% frequency points of the SFHS. Then, target position estimation is conducted with both SFHSs and PRFHSs. Comparable position estimation results are obtained, which show the effectiveness of the proposed method. Benefiting from the wide analog bandwidth of the proposed MPSDR, SFHSs can be directly replaced with PRFHSs, which can not only achieve comparable performance but also enhance scanning and measurement speed and improve anti-jamming capability.

2. Principle

Figure 1(a) illustrates the schematic of the proposed radar, which consists of an FH signal transmitter and an MPSDR. The signal generated by the radio-frequency (RF) source can be denoted as

$$s(t) = \sum_{i=0}^{N-1} \operatorname{rect}\left(\frac{t - iT_r}{T_r}\right) A(f_{RF,i}) \cos(2\pi f_{RF,i}t + \varphi_i), \quad (1)$$

where $\operatorname{rect}(x)$ is given by $\operatorname{rect}(x) = 1$, $|x| \le 0.5$; 0, |x| > 0.5, T_r , $A(f_{RF,i})$, and φ_i are the duration, amplitude, and initial phase of the signal at the *i*th hopped frequency $f_{RF,i}$, respectively. Then, the generated signal is split into two branches by a power divider, one branch serving as the reference signal and the other as the measurement signal. The measurement signal is radiated

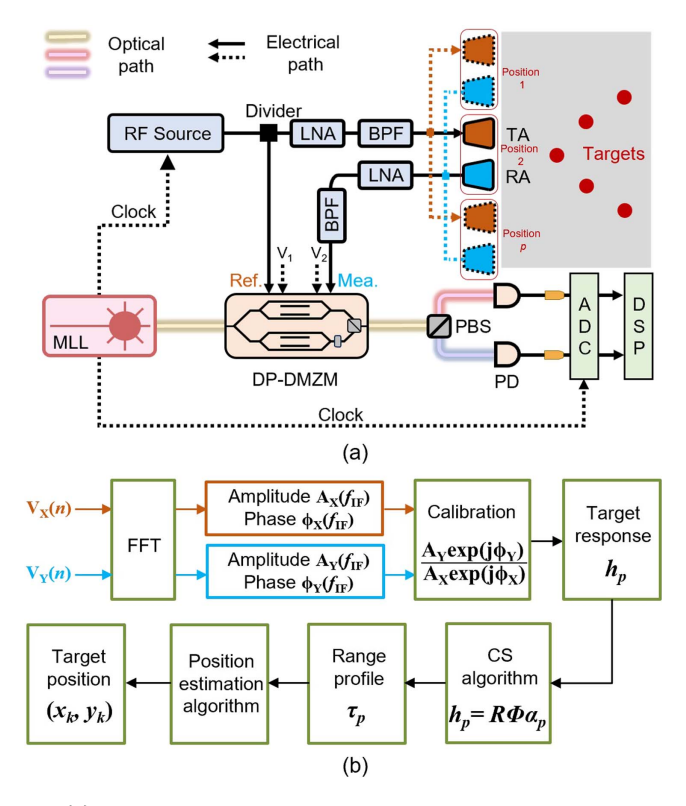


Fig. 1. (a) Schematic diagram of the proposed radar. MLL, mode-locked laser; DP-DMZM, dual-polarization dual-drive Mach-Zehnder modulator; PBS, polarization beam splitter; PD, photodetector; ADC, analog-to-digital converter; DSP, digital signal processing; LNA, low-noise amplifier; BPF, bandpass filter; TA, transmit antenna; RA, receive antenna. (b) DSP procedures. FFT, fast Fourier transform; CS, compressed sensing.

by the transmit antenna (TA) after being amplified and filtered by a low-noise amplifier (LNA) and a bandpass filter (BPF), respectively. Thus, the radar echo reflected by K scatterers is received by the receive antenna (RA). Both the reference signal and the echo are collected by the microwave photonic subsampling digital receiver. For simplicity in analysis, only the signal at frequency $f_{\rm RF}$ is considered. Consequently, the received signals can be expressed as

$$\begin{bmatrix} s_{\text{ref}}(t) \\ s_{\text{echo}}(t) \end{bmatrix} = \begin{bmatrix} A_1(f_{RF})\cos(2\pi f_{RF}t + \varphi_1) \\ A_2(f_{RF})\sum_{i=1}^{K} r_i \cos[2\pi f_{RF}(t - \tau_i) + \varphi_2] \end{bmatrix}, (2)$$

where $A_1(f_{RF})$ and $A_2(f_{RF})$ are the amplitudes of the reference and echo signals, respectively, r_i and τ_i represent the reflected coefficient and delay of the *i*th scatter, and φ_1 and φ_2 denote the signal phases.

In the MPSDR, the optical pulses for sampling are generated by an MLL, which can be given as

$$E_{\text{MLL}}(t) = \sqrt{P} \sum_{n=-\infty}^{+\infty} \delta(t - nT_s) = \sqrt{P} \sum_{n=-\infty}^{+\infty} a_n e^{j2\pi n f_{\text{rep}} t}, \quad (3)$$

where P represents the peak power of the optical pulses, and T_s , $f_{\rm rep}$, and a_n denote the pulse period, repetition rate, and Fourier series coefficients, respectively. The reference and echo signals drive the two sub-DMZMs of a DP-DMZM in orthogonal polarization states, with small signal modulation and both sub-DMZMs biased at the quadrature transmission point (QTP). Therefore, the output of the DP-DMZM can be given as

$$\begin{bmatrix} E_X(t) \\ E_Y(t) \end{bmatrix} \propto \frac{\sqrt{2}}{2} \begin{bmatrix} 1 + \frac{\pi s_{\text{ref}}(t)}{V_{\pi X}} \\ 1 + \frac{\pi s_{\text{ech}}(t)}{V_{\pi Y}} \end{bmatrix} E_{\text{MLL}}(t), \tag{4}$$

where $V_{\pi X}$ and $V_{\pi Y}$ denote the half-wave voltage of the two sub-DMZMs, respectively. The output optical pulses are directed into two paths along orthogonal polarization directions by a polarization beam splitter (PBS). Notably, the two orthogonal polarization states of the PBS are aligned with those of the DP-DMZM, assuming the frequency of the modulated RF signal is $f_{\rm RF} = f_{\rm IF} + R(N)f_{\rm rep}$, where $f_{\rm IF}$ is the intermediate frequency located within the first Nyquist region and R(N) is an integer. After photoelectric detection by two photodetectors (PDs), the optical pulses from both paths are converted to electrical signals and captured by two ADCs with a sampling period of T_s . The digitized signals at frequency $f_{\rm IF}$ can then be given as

$$\begin{bmatrix} V_X(n) \\ V_Y(n) \end{bmatrix} \propto \begin{bmatrix} H_X(f_{RF}) \cos[2\pi f_{IF} n T_s + \varphi_X(f_{RF})] \\ H_Y(f_{RF}) \sum_{i=1}^K r_i \cos[2\pi f_{IF} n T_s - 2\pi R(N) f_{rep} \tau_i + \varphi_Y(f_{RF})] \end{bmatrix},$$
(5)

where *n* represents the index of the sampling sequence, $H_X(f_{RF})$, $\varphi_X(f_{RF})$ and $H_Y(f_{RF})$, $\varphi_Y(f_{RF})$ are the amplitude and phase

responses at $f_{\rm RF}$ for the reference and measurement paths, respectively. It is worth noting that $H_Y(f_{\rm RF})$ and $\varphi_Y(f_{\rm RF})$ are related to the measurement system and are independent of the targets. Figure 1(b) depicts the digital signal-processing procedures applied to $V_X(n)$ and $V_Y(n)$. The FFT is first performed to extract the amplitude $A_X(f_{\rm IF})$, $A_Y(f_{\rm IF})$ and phase $\phi_X(f_{\rm IF})$, $\phi_Y(f_{\rm IF})$ at $f_{\rm IF}$ of $V_X(n)$ and $V_Y(n)$, respectively. Then, the calibration process is adopted to eliminate the influence of the reference path, which can be given as

$$h_{\text{mea}} = \frac{A_Y(f_{\text{IF}})e^{j\phi_Y(f_{\text{IF}})}}{A_X(f_{\text{IF}})e^{j\phi_X(f_{\text{IF}})}} = \frac{H_Y(f_{\text{RF}})e^{-j\varphi_Y(f_{\text{RF}})}}{H_X(f_{\text{RF}})e^{-j\varphi_X(f_{\text{RF}})}} \sum_{i=1}^K r_i e^{j2\pi R(N)f_{\text{rep}}\tau_i}.$$
(6)

Furthermore, the impact of the entire measurement system response can be further removed by performing a direct connection measurement between the two antennas. The target response can be obtained by

$$h_{\text{tar}} = \frac{h_{\text{mea}}}{h_{\text{sys}}} = \sum_{i=1}^{K} \alpha_i e^{j2\pi R(N)f_{\text{rep}}\tau_i},$$
 (7)

where $h_{\rm sys}$ is the relative system response at $\tau_i=0$ in Eq. (6), and α_i denotes the relative reflected intensity of ith scatter. Figure 2(a) illustrates a frequency grid formed by a total of N uniformly spaced frequencies with an interval $f_{\rm rep}$. Assuming M (where $M \leq N$) frequencies are pseudo-randomly selected from the grid, as shown in Fig. 2(b), these M frequencies define the hopping sequence for the PRFHS. The frequency of the Mth hop can be expressed as $f_{\rm RF}=f_{\rm IF}+R(M)f_{\rm rep}$. Consequently, a target response vector can be obtained from the responses at these M frequency points, which can be represented as

$$\mathbf{h} = \left[\sum_{i=1}^{K} \alpha_i' e^{j2\pi R(1)f_{\text{rep}}\tau_i} \quad \dots \quad \sum_{i=1}^{K} \alpha_i' e^{j2\pi R(M)f_{\text{rep}}\tau_i} \right]^T = \mathbf{R}\mathbf{\Phi}\alpha,$$
(8)

where **R** denotes the measurement matrix to randomly select M rows of Φ , Φ is the inverse discrete Fourier transform (IDFT) matrix, and α is the relative reflected coefficient vector. The dimensions of **R**, Φ , and α are $M \times N$, $N \times N$, and $N \times 1$, respectively. In addition, most radar detection scenarios can

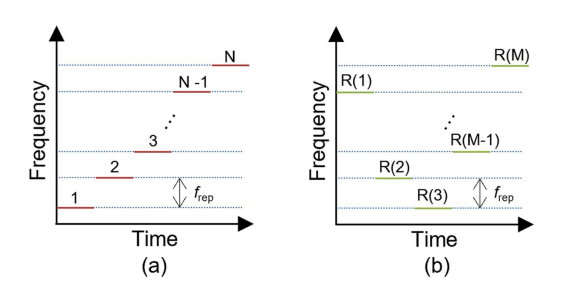


Fig. 2. (a) Frequency grid formed by N uniformly spaced frequencies. (b) Signal with M pseudo-randomly selected frequencies.

be viewed as multiple individual scatterers. Therefore, the echo signals can satisfy the signal sparsity requirement of compressed sensing (CS) theory^[12], which indicates that α is K sparse. Thus, α can be solved by an l_1 minimization problem,

$$\hat{\mathbf{\alpha}} = \arg \min \|\mathbf{\alpha}\|_1 \quad \text{s.t. } \mathbf{h} = \mathbf{R}\mathbf{\Phi}\mathbf{\alpha}.$$
 (9)

Consequently, the target responses corresponding to the N grid frequencies can be reconstructed from the target responses obtained from the M randomly selected frequency hops using the orthogonal matching-pursuit (OMP) algorithm^[13]. Then, the range profile τ can be derived by applying inverse fast Fourier transform (IFFT) to $\Phi\alpha$.

To estimate the target positions, several measurement positions are performed on the antenna pair, and the corresponding range profile τ_p can be collected with the measurement position \mathbf{p} . Therefore, the backprojection (BP) algorithm with multiplicative tomography weighting (MTW) can be adopted to obtain the range profiles to determine the coordinates of prominent scatterers in a 2D image^[14]. The amplitude at the image pixel (x, y) can be expressed as

$$A(x,y) = \prod S(\tau_p), \tag{10}$$

where $S(\tau_p)$ represents the result of interpolating the pixel amplitudes of the 2D image onto the 1D range profile τ_p . Then, target positions can be estimated by identifying the peak pixels.

3. Experimental Results

A demonstrated experiment based on the setup depicted in Fig. 1(a) is carried out. The optical pulse source is an MLL (Calmar, FPL-01) with a 10-MHz repetition frequency. The MLL generates optical pulses with a width of approximately 380 fs and a power of 18 dBm. These optical pulses are directed into a DP-DMZM (Fujitsu, FTM7980) with polarization-maintaining input and output fibers. The DP-DMZM is driven by the reference and the radar echo signals. Each sub-DMZM is biased at QTP. Then, a PBS is used to separate the optical pulses with orthogonal polarization states into two branches. Photoelectric detection is implemented at two branches using two PDs (CETC, GD45227R) with a responsivity of 0.8 A/W. The input optical power of the PD is about 4 dBm. Following this, the IF signal acquisition is performed by a 14-bit dual-channel ADC (Teledyne SPD, ADQ14) after filtering through an LPF with a cutoff frequency of 5 MHz. The sampling rate of the ADC is 10 MSa/s and is synchronized with the repetition frequency of the MLL.

A microwave source (R&S, SMA100B) is used as the FH signals generator. The frequency of the output microwave signal can be programmed to be hopped over time. In the experiments, a frequency grid ranging from 18.001 to 26.001 GHz is used, with 10 MHz intervals, resulting in a total of 801 frequency points. Therefore, the frequency $f_{\rm RF,i}$ in Eq. (1) can be expressed

as $f_{\rm RF,i}=f_{\rm IF}+if_{\rm rep}$, where $i=1800,1801,1802,\ldots,2600$ and $f_{\rm IF}$ is 1 MHz. The output power of the microwave source is set to 10 dBm. The generated FH signals are first split into two branches by a power divider. One branch directly drives one input of the DP-DMZM, while the other is radiated by a TA (A-info, LB1840). The echo signals are received by an RA and drive the other input of the DP-DMZM. Both the transmitted and received signals are amplified and filtered by an 18–26 GHz LNA and an 18–26 GHz BPF, respectively.

To verify the effectiveness of the proposed method for range profile detection, experiments are conducted based on an SFHS with N=801 hops and a PRFHS with M=100 hops. The FH sequences are, respectively, shown in Figs. 3(a) and 3(b). Figure 4 shows the experimental scene and results. The target scene is illustrated in Fig. 4(c), where the targets consist of three bolts, spaced 7.5 and 2.5 cm apart, and can be considered sparse targets. First, an SFHS-based experiment is carried out; Fig. 4(a)

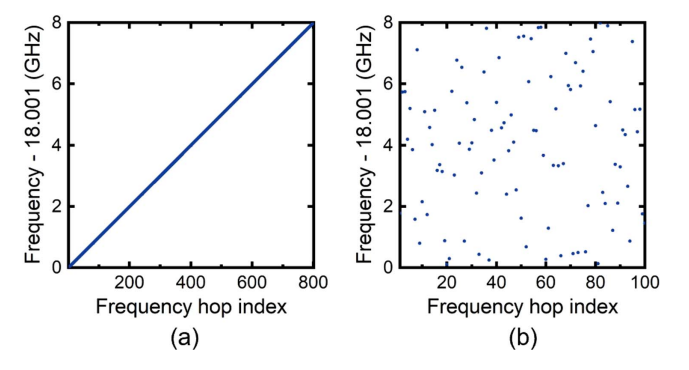


Fig. 3. Frequency profiles of the frequency-hopping sequences. (a) SFHS. (b) PRFHS.

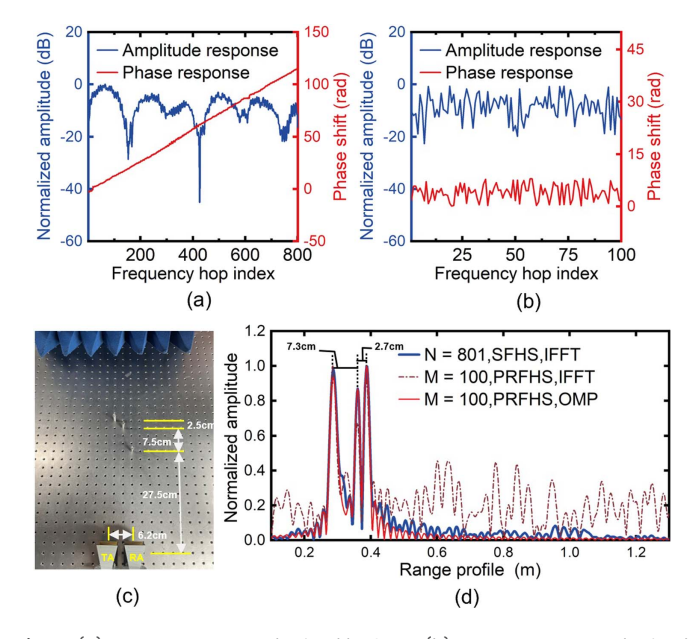


Fig. 4. (a) Target responses obtained by SFHP. (b) Target responses obtained by PRFHP. (c) Target scene for range profile measurement. (d) Range profiles obtained by SFHP and PRFHP.

shows the amplitude and phase responses of the targets when the SFHS is employed. The range profile can then be derived by applying the IFFT to the responses, as shown by the blue solid line in Fig. 4(d). As can be seen, the high-resolution range profile of the targets is successfully acquired with distances between the targets calculated to be 7.3 and 2.7 cm. Then, the PRFHS is adopted; the detected target responses are shown in Fig. 4(b). It can be seen that the randomness of the target responses makes it fail to directly obtain the range profile through IFFT. Therefore, reordering based on the measurement matrix R is performed to the target responses, and the range profile is successfully obtained after IFFT, as the red dashed line in Fig. 4(d) shows. However, severe spurs are observed in the red dashed range profile. Fortunately, the reliable range profile can be acquired by processing the target responses with Eqs. (8) and (9). As shown by the red solid line in Fig. 4(d), the range profile is successfully reconstructed. This approach achieves a reconstruction accuracy comparable to that of the SFHS, with 12.5% of the frequency points.

In the target position estimation experiment, the same signals are used. As shown in Fig. 5(a), the targets consist of five bolts arranged in a V-shape. Then, multiple range profiles are measured by changing the measurement position of the antenna pair. The antenna pair positions are listed in Table 1. Figure 5(b) shows the range profiles measured at three of these positions

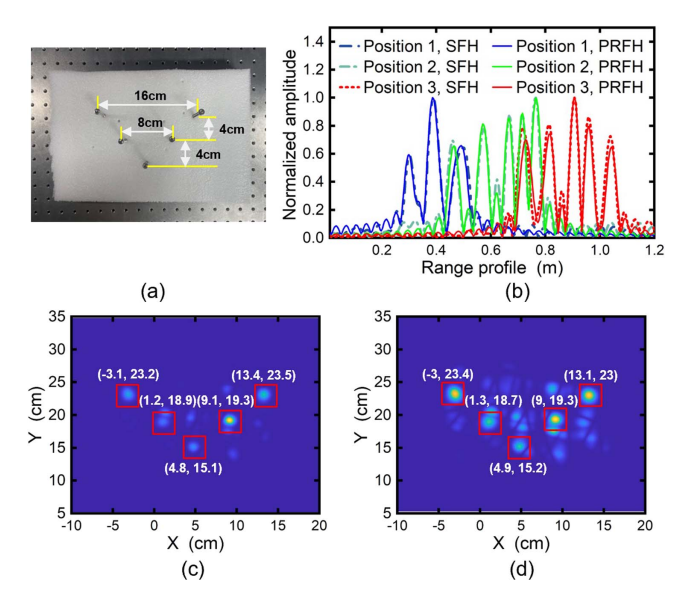


Fig. 5. (a) Target scene for position estimation. (b) Range profiles obtained by SFHP and PRFHP. Position estimation results obtained by SFHP (c) and PRFHP (d), respectively.

Table 1. Coordinates of the Antenna Pairs.

TA (cm)	(0, 0)	(25, 30)	(50, 30)	(50, 20)	(10, 55)	(20, 55)
RA (cm)	(6.2, 0)	(25, 36.2)	(50, 23.8)	(50, 13.8)	(16.2, 55)	(26.2, 55)

using the SFHS and PRFHS. It can be seen that the range profiles are successfully reconstructed. Therefore, a 2D image of the target positions can be obtained using the BP algorithm with MTW. The target coordinates are then derived by searching for the peak pixels. The position estimation results for the SFHS and PRFHS are shown in Figs. 5(c) and 5(d), respectively. Notably, the accuracy of the PRFHS, utilizing only 12.5% of the frequency points of SFHS, is comparable for sparse target position estimation. The employment of sparse FH signals can significantly reduce the number of frequency points, thereby increasing the measurement speed of the system.

It should be noted that the sampling rate of the proposed MPSDR is consistent with the minimum frequency-hopping interval. As the hopping interval decreases, the required sampling rate can be decreased, and the unambiguous range can also be increased. In addition, the frequency range of the FH signal can be further expanded, which is only confined by the bandwidth of the DP-DMZM.

4. Conclusion

In conclusion, an MPSDR that can direct sample and process FH signals with complex frequency profiles for target position estimation is proposed and experimentally demonstrated. An 801-hopped SFHS and a 100-hopped PRFHS with frequencies across 18 to 26 GHz are successfully captured and processed by the proposed MPSDR, and comparable target position estimation results are obtained. The employment of the PRFHS can significantly reduce the number of frequency points, thereby increasing the measurement speed. The proposed MPSDR has a simple structure, high integrability, and broad compatibility with various types of FH signals. The performance could be further enhanced using an integrated MPSDR and broadband FH signals.

Acknowledgements

This work was supported by the Innovation Capacity Building Plan (Science and Technology Facilities) of Jiangsu (No. BM2022017) and the Fundamental Research Funds for the Central Universities (No. NI023003).

References

- N. T. Hung, F. F. C. Rego, and A. M. Pascoal, "Cooperative distributed estimation and control of multiple autonomous vehicles for range-based underwater target localization and pursuit," IEEE Trans. Contr. Syst. Technol. 30, 1433 (2022).
- 2. M. Skolnik, Radar Handbook (McGraw-Hill, 2008).
- W. Yi and P. K. Varshney, "Adaptation of frequency hopping interval for radar anti-jamming based on reinforcement learning," IEEE Trans. Veh. Technol. 71, 12434 (2022).
- C. Ma, Y. Yang, F. Cao, et al., "High-resolution microwave photonic radar with sparse stepped frequency chirp signals," IEEE Trans. Geosci. Remote Sens. 60, 1 (2022).
- K. Wu, J. A. Zhang, X. Huang, et al., "Frequency-hopping MIMO radarbased communications: an overview," IEEE Aerosp. Electron. Syst. Mag. 37, 42 (2022)
- A. Li, H. Huan, R. Tao, et al., "Implementation of mixing sequence optimized modulated wideband converter for ultra-wideband frequency hopping signals detection," IEEE Trans. Aerosp. Electron. Syst. 56, 4698 (2020).
- 7. B. C. Pile and G. W. Taylor, "Performance of subsampled analog optical links," J. Lightwave Technol. 30, 1299 (2012).
- P. Ghelfi, F. Laghezza, F. Scotti, et al., "A fully photonics-based coherent radar system," Nature 507, 341 (2014).
- D. R. Reilly, S. X. Wang, and G. S. Kanter, "Nonuniform optical undersampling for high-resolution microwave frequency measurements," IEEE Photon. Technol. Lett. 24, 997 (2012).
- X. Li, A. Wen, X. Li, et al., "Wideband RF subsampling and disambiguation based on phase shift analysis," J. Lightwave Technol. 40, 1027 (2022).
- X. Li, A. Wen, X. Li, et al., "Wideband frequency and angle-of-arrival measurement system based on optical subsampling," IEEE Trans. Microw. Theory Technol. 71, 784 (2023).
- S. Liu, S. Wang, T. Shi, et al., "Photonics-assisted compressed sensing radar receiver for frequency domain non-sparse signal sampling based on dictionary learning," Opt. Lett. 48, 767 (2023).
- J. A. Tropp and A. C. Gilbert, "Signal recovery from random measurements via orthogonal matching pursuit," IEEE Trans. Inform. Theory 53, 4655 (2007)
- G. Sun, F. Zhang, and S. Pan, "Photonic-assisted high-resolution incoherent back projection synthetic aperture radar imaging," Opt. Commun. 466, 125633 (2020).